Progressive Damage Model of Carbon-fiber Reinforced Polymer Laminates under Low-velocity Impact Loading

Mohd Suhairil Meon[*], *Muhammad Faizul Iqmal Mordi*, *Jamaluddin Mahmud*
School of Mechanical Engineering, College of Engineering,
Universiti Teknologi MARA, 40450 Shah Alam, Selangor, MALAYSIA
**msuhairil@uitm.edu.my*

ABSTRACT

The study quantitatively investigates the mechanical structural behavior and damage mechanisms of composite laminates under low-velocity impacts using Abaqus software. A three-dimensional Puck criterion is utilized to identify the onset of fiber failure and matrix cracking under tensile and compressive loading conditions. Two progressive damage evolution models are implemented to simulate damage propagation during impact. The model also incorporates cohesive elements with a bilinear traction-separation law to represent interlaminar damage. The performance of the model is validated by comparing its predictions against experimental results for a composite laminate with a stacking sequence of [0°₃/45°/-45°₂/45°/0°₃] subjected to different impact energies (2 J, 4 J, and 8 J). Despite a slight reduction in accuracy at higher energy levels, the model effectively predicts force-displacement curves and energy absorption. The deviation from experimental results is approximately ±6%. This research offers a basis for enhancing the impact resistance and energy absorption characteristics of composite materials.

Keywords: *Composite Laminates; Finite Element Analysis; Low-Velocity Impact; Progressive Damage Model*

ISSN 1823-5514, eISSN 2550-164X

https://doi.org/10.24191/jmeche.v13i1.2844

Received for review: 2024-06-17
Accepted for publication: 2024-09-23
Published: 2024-11-15

Introduction

Composite laminates have been widely utilized across various engineering disciplines such as automotive, aerospace, marine, and defense sectors due to their favourable lightweight properties and high strength-to-weight ratio. However, their susceptibility to impact loading presents a significant challenge that can compromise their otherwise superior performance. Low-Velocity Impact (LVI) events, characterized by relatively low kinetic energy, are particularly concerning as they can diminish the material's stiffness and overall strength [1]. The insidious nature of this damage mechanism lies in its often-undetectable nature. Unlike readily visible surface cracks, LVI-induced damage can remain hidden within the laminate, posing a serious threat to structural integrity.

In response to this critical issue, a substantial body of research has been devoted to understanding LVI behavior in composites. These efforts have employed various methodologies, including experimental testing [2]–[3], numerical simulations [4]–[6], and even combined approaches that leverage both experimental data and computational modelling [7]–[10]. Notably, advancements in computing power have propelled the finite element method (FEM) as the more robust and cost-saving for numerically predicting LVI failure in composite laminates.

Numerical approaches have emerged as a prominent tool for investigating LVI behavior. Studies by Zhou et al. [11], Falcó et al. [12], Ao et al. [13], Joglekar et al. [14], Nagaraj et al. [15], Meon et al. [16], and Zhou et al. [17] have all employed numerical methods to examine the impact response of composites. These studies explored the influence of factors such as lamination scheme, material properties, and impactor characteristics on the extent of damage (both intra and interlaminar) and the structural response of the laminates. Furthermore, research has investigated the effectiveness of different modelling techniques used in Finite Element Analysis (FEA) for simulating LVI damage in composites. Sridharan and Pankow [18] evaluated various FEA methods for characterizing different impact scenarios, while Zhao and Zhou [19] studied the changes in structural integrity based on single and multiple impact events on the composite laminates.

Material characterization has been an important area of investigation. For instance, Meon et al. [20] analysed the characteristic of impact and failure patterns of composite laminates, focusing on the interactions between the fiber and matrix elements. Several studies have specifically addressed the onset and progression of damage within the laminate structure. Zhou et al. [21] examined the development of intra and interlaminar damage under LVI in cross-ply laminates. Similarly, Li et al. [22] assessed the suitability of various failure theories and damage progression models for the FEA of LVI-impacted composites. Beyond laminates, research has also extended to composite structures. Liao and Jia [23] investigated the failure processes and dynamic

response of composite pressure vessels subjected to LVI. Liao et al. [24] further analysed the accumulation of damage behavior based on LVI on composite laminate. Additionally, Maio et al. [6] examined the delamination damage at the interlaminar interface of fiber-reinforced composites under LVI.

Predicting the damage initiation and progression is crucial for a detailed LVI modelling strategy. This requires the execution of a progressive failure model for composite plies, comprising both failure criteria and damage progression criteria. 3D Hashin failure criteria [25] have received significant attention in previous research as initiation criteria for identifying failure, particularly in unidirectional (UD) composite laminates. This corresponds to its efficacy in isolating different failure modes. Long et al. [26] and Tie et al. [27] employed the Hashin formulation with a linear degradation scheme as a progression law for LVI failure analysis. Additionally, Tie et al. [2] successfully predicted impact-induced failure in laminates using 3D Hashin damage criteria coupled utilising a Continuum Damage Mechanics (CDM) damage evolution law, demonstrating a similar trend with experimental results. Furthermore, the combination of Hashin [25] and Puck criteria [28] for predicting failures due to fibre fracture and interfiber cracking is a frequently encountered approach in several research articles [4], [10], [28]. This leverages the strengths of both criteria for a more comprehensive assessment. To exploit the capabilities of modern computing power, a numerical investigation of LVI failure analysis was also conducted employing micromechanics failure criteria (MMF) [7]-[9].

This study evaluated the structural behaviour and failure characteristics of laminated composites subjected to LVI using a combined approach of impact energy analysis and a developed progressive damage model. Laminate samples were assessed for their impact response and progressive damage progression under a varied range of impact energies. A solid 3D Finite Element (FE) model was developed within the ABAQUS/Explicit program to simulate the composite material. The VUMAT subroutine, coded in FORTRAN, was implemented within the simulation. The Puck failure criterion with different degradation laws was employed to analyse intralaminar damage, while cohesive elements were used to investigate interlaminar damage. The study gathered data on the structural behavior of the Carbon Fibre fiber-reinforced polymer (CFRP) composite system, encompassing force, displacement, and energy absorption under different impact energy levels. The evaluation highlighted areas of fiber and inter-fiber damage within individual layers and examined interfacial failure or delamination occurring between the layers.

Methodology

Intralaminar progressive damage model

This sub-section introduces the progressive damage model that has been chosen for the composite laminate. The 3D Puck failure criteria [28] were selected to precisely detect the onset of damage, with a specific focus on differentiating between fibre and inter-fiber failure in both tension and compression. Expanding on Hashin's criterion [25], Puck's framework offers a more comprehensive approach. The governing equations for fiber failure (FF) within the laminate are presented in Equations (1) and (2):

Fiber Failure (FF) in tension:

$$FF_t = \frac{1}{X_t}\left[\sigma_{11} - \left(v_{12} - v_{12f}\left(m_{\sigma f}\frac{E_1}{E_{1f}}\right)\right)(\sigma_{22} + \sigma_{33})\right] \text{for } [\dots] \geq 0 \quad (1)$$

FF in compression:

$$FF_c = -\frac{1}{X_c}\left[\sigma_{11} - \left(v_{12} - v_{12f}\left(m_{\sigma f}\frac{E_1}{E_{1f}}\right)\right)(\sigma_{22} + \sigma_{33})\right] \text{for } [\dots] < \quad (2)$$

For unidirectional (UD) composite plies, longitudinal tensile and compressive strengths are designated by X_t and X_c, respectively. Poisson's ratios of the unidirectional lamina and its fibers are ν_{12} and ν_{12f}, respectively, with ν_{12} commonly assumed to be 0.33. To account for fiber-specific behavior, a mean stress magnification factor ($m_{\sigma f}$) of 1.1 is used for CFRP composites, and the fiber's Young's modulus (E_{1f}) is set at 230 GPa.

Complementing the UD ply properties, Inter-Fiber Failure (IFF), or matrix cracking, arises within a laminate due to stresses exerted on the plane of fracture. These stresses encompass normal stress (σ_n), longitudinal shear stress (τ_{nl}), and transverse shear stress (τ_{nt}), each inclined at an angle θ relative to the material plane. Classical transformation equations, which account for the FP's orientation and direction, are employed to calculate these stresses. By transforming stresses from the material plane to the FP, these equations enable a more precise evaluation of IFF value. The IFF function is formulated based on the stresses acting on the FP, facilitating the prediction and comprehension of matrix cracking behavior in composite laminates. The governing equations for IFF are presented as:

Inter-fiber failure (IFF) in tension:

$$IFF_t(\theta) = \sqrt{\left(\left(\frac{1}{R_\perp} - \frac{P^+_{\perp\psi}}{R_{\perp\psi}}\right)\sigma_n(\theta)\right)^2 + \left(\frac{\tau_{nt}(\theta)}{R_{\perp\perp}}\right)^2 + \left(\frac{\tau_{nl}(\theta)}{R_{\perp\parallel}}\right)^2} + \frac{P^+_{\perp\psi}}{R_{\perp\psi}}\sigma_n(\theta) \text{ for } \sigma_n \geq 0 \tag{3}$$

Inter-fiber failure (IFF) in compression:

$$IFF_c(\theta) = \sqrt{\left(\frac{P^-_{\perp\psi}}{R_{\perp\psi}}\sigma_n(\theta)\right)^2 + \left(\frac{\tau_{nt}(\theta)}{R_{\perp\perp}}\right)^2 + \left(\frac{\tau_{nl}(\theta)}{R_{\perp\parallel}}\right)^2} + \frac{P^-_{\perp\psi}}{R_{\perp\psi}}\sigma_n(\theta) \quad \text{for } \sigma_n < 0 \tag{4}$$

with:

$$R_\perp = Y_t;\ R_{\perp\parallel} = S_{21};\ R_{\perp\perp} = \frac{Y_c}{2(1 + P^-_{\perp\perp})} \tag{5}$$

and:

$$\begin{gathered} \frac{P^+_{\perp\psi}}{R_{\perp\psi}} = \frac{P^+_{\perp\perp}}{R_{\perp\perp}}cos^2\psi + \frac{P^+_{\perp\parallel}}{R_{\perp\parallel}}sin^2\psi \\ \frac{P^-_{\perp\psi}}{R_{\perp\psi}} = \frac{P^-_{\perp\perp}}{R_{\perp\perp}}cos^2\psi + \frac{P^-_{\perp\parallel}}{R_{\perp\parallel}}sin^2\psi \\ cos^2\psi = \frac{\tau^2_{nt}(\theta)}{\tau^2_{nt}(\theta) + \tau^2_{nl}(\theta)};\ sin^2\psi = \frac{\tau^2_{nl}(\theta)}{\tau^2_{nt}(\theta) + \tau^2_{nl}(\theta)} \end{gathered} \tag{6}$$

The symbol ψ represents the shear orientation within the plane of action, which plays a vital role in capturing the influence of in-plane shear stresses. Furthermore, $R_\perp$ represents the failure resistance specifically for stresses acting normal to the fiber direction. To reflect the complex shear behavior within the action plane, the criteria incorporate $R_{\perp\psi}$, $R_{\perp\perp}$, and $R_{\perp\parallel}$, which correspond to the fracture resistances for shear in the ψ, normal, and parallel directions, respectively. These parameters represent the fracture resistances of the action plane due to shear stressing in the ψ, normal, and parallel directions, respectively. Moreover, Y_t and Y_c indicate the transverse tensile and compressive strengths, while S_{21} represents the in-plane shear strength of the laminate. Further details on the associated Puck inclination parameters are summarized in Table 1.

Table 1: Recommended Puck's parameters

Type	Inclination parameter (-)			
	$P_{\perp\parallel}^{+}$	$P_{\perp\parallel}^{-}$	$P_{\perp\perp}^{+}$	$P_{\perp\perp}^{-}$
GFRP	0.3	0.25	0.2 - 0.25	0.2 - 0.25
CFRP	0.35	0.3	0.25 - 0.3	0.25 - 0.3

Glass fibre reinforced polymer (GFRP); Carbon fibre reinforced polymer (CFRP)

To simulate the elastic-brittle behavior characteristic of fiber-reinforced composites, this study adopts a constitutive model specifically designed for composite materials. This selection aligns with the successful application of a similar numerical model by Lee et al. [29] for identifying both failure initiation and damage evolution. The core of this model is a 3D-damaged stiffness matrix, expressed mathematically as:

$$C^{d} = \begin{bmatrix} \beta C_{11} & \kappa C_{12} & \kappa C_{13} & 0 & 0 & 0 \\ \kappa C_{21} & \kappa C_{22} & \kappa C_{23} & 0 & 0 & 0 \\ \kappa C_{31} & \kappa C_{32} & \kappa C_{33} & 0 & 0 & 0 \\ 0 & 0 & 0 & \beta\omega G_{12} & 0 & 0 \\ 0 & 0 & 0 & 0 & \beta\omega G_{13} & 0 \\ 0 & 0 & 0 & 0 & 0 & \beta\omega G_{23} \end{bmatrix} \tag{7}$$

where C_{ij} represents the undamaged stiffness components, and G_{12}, G_{13}, and G_{23} denote the in-plane and out-of-plane shear moduli of the composite material. The damage factors β, κ, and ω are defined as follows:

$$\begin{aligned} \beta &= 1 - d_f \\ \kappa &= \big(1 - d_f\big)(1 - d_m) \\ \omega &= (1 - S_{mt} d_{mt})(1 - S_{mc} d_{mc}) \end{aligned} \tag{8}$$

To quantify damage progression, the model incorporates global damage variables, d_f and d_m, representing fiber and inter-fiber failure, respectively. These global variables further decompose into individual damage variables, d_{ft}, d_{fc}, d_{mt}, and d_{mc}. The individual variables capture damage due to tension (*ft*, *mt*) and compression (*fc*, *mc*) for each failure mode. The correlation between global and local factors is established as $d_f = 1 - \big(1 - d_{ft}\big)\big(1 - d_{fc}\big)$ and $d_m = 1 - (1 - d_{mt})(1 - d_{mc})$ account for the cumulative nature of damage, ensuring that the overall damage state reflects the combined effects of individual damage mechanisms. Control parameters, $S_{mt} = 0.9$ and $S_{mc} = 0.5$, influence this interaction between local damage variables, as explained in the Abaqus manual.

The damage progression criteria employed in this article are summarized in Table 2. Two progression criteria (GD1 and GD2) are utilized. When an activation function reaches unity for a specific local damage variable of d_{ft}, d_{fc}, d_{mt}, or d_{mc} corresponding to a particular failure mode (tension/compression), the damage is activated. Consequently, the damaged stiffness matrix is recalculated, leading to an updated stress state. The index *i* denotes the direction (tension or compression), while the factor *m* is typically set to 1.

Table 3: Activation functions and gradual degradation schemes used in this publication [16]

Activation function	**Gradual Degradation (GD) function**	
	GD 1	**GD 2**
$FF_i > 1$	$d_{fi} = 1 - e^{\left[\frac{1}{m}(1-FF_i)\right]}$	$d_{fi} = \frac{1}{FF_i}$
$IFF_i > 1$	$d_{mi} = 1 - e^{\left[\frac{1}{m}(1-IFF_i)\right]}$	$d_{mi} = \frac{1}{IFF_i}$

Interlaminar progressive damage model

Low-velocity impacts can induce delamination, which is a critical form of damage within composite materials that often remains undetectable by visual inspections. To capture this interface debonding, Abaqus/Explicit built-in cohesive elements are utilized. Cohesive element interfaces are employed to simulate delamination, the primary interlaminar damage mode.

Formulated through a fracture-separation law, this approach governs the relationship between traction stress and separation displacement within the model, as expressed in the following form:

$$t = \begin{bmatrix} t_n \\ t_s \\ t_t \end{bmatrix} = \begin{bmatrix} K_{nn} & 0 & 0 \\ 0 & K_{ss} & 0 \\ 0 & 0 & K_{tt} \end{bmatrix} \begin{bmatrix} \delta_n \\ \delta_s \\ \delta_t \end{bmatrix} \tag{9}$$

In this context, t_n, t_s, and t_t represent the interfacial strength corresponding to damage modes I, II, and III respectively.

Table 4 summarizes the key cohesive law parameters: interface strength, t_i^o (i = n, s, t), and critical fracture energy, G_i^c (i = n, s, t). These parameters define the material's resistance to separation and energy absorption before failure in normal and shear directions. The B-K parameter η is typically set to 1.45. Delamination initiates when a quadratic function reaches unity, signifying damage criterion fulfilment.

Table 5: Failure criteria used for interlaminar damage [16]

Phase	Criteria
Damage initiation	Quadratic nominal stress criterion $\left\{\frac{\langle t_n \rangle}{t_n^o}\right\}^2 + \left\{\frac{t_s}{t_s^o}\right\}^2 + \left\{\frac{t_t}{t_t^o}\right\}^2 = 1$
Damage progression	B-K criterion $G^C = G_n^C + (G_s^C - G_n^C)\left\{\frac{G_S}{G_T}\right\}^\eta$

Numerical model

A finite element model was created to examine the low-velocity impact (LVI) attributes of the composite laminate. The laminate had dimensions of 87.5 mm × 65 mm × 3.2 mm, arranged according to the stacking sequence shown in Figure 1. A rigid, semicircular impactor measuring 12.5 mm in diameter and weighing 2.34 kg was used to simulate the impact. Three different impact energy levels (2 J, 4 J, and 8 J) were tested by setting the initial velocities of the impactor to 1.3 m/s, 1.84 m/s, and 2.61 m/s, respectively. The interaction of impactor laminate was modelled using surface-to-surface contact through a friction coefficient of 0.3.

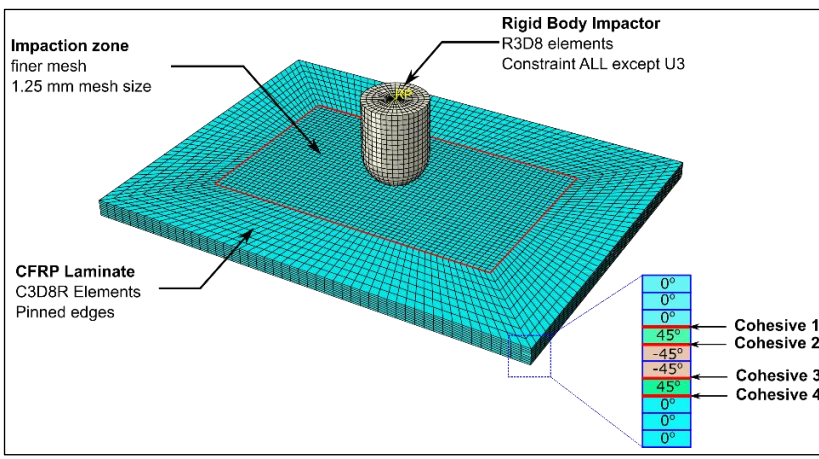

Figure 1: Specifications of the FEM for LVI simulation

The laminate was discretised utilising eight-node, three-dimensional reduced-integration elements (C3D8R), with each layer measuring 0.32 mm in thickness. To guarantee accurate results and prevent excessive element distortion, the distortion control option was activated, ensuring computational

stability. The material properties of the HS300/ET223 composite material are provided in Table 6. To capture delamination behavior, eight-node cohesive elements (COH3D8) with finite-thickness of 0.001 mm were inserted between laminate layers at varying angles. Notably, a maximum stiffness reduction of 1 was employed, and failed elements were retained in the analysis. This approach facilitates a comprehensive evaluation of delamination phenomena within the composite structure.

Table 7: Intra- and interlaminar properties of the HS300/ET223 UD composite laminate [30]

Intralaminar properties		
Density		1600 kg/m³
Elastic	Young's modulus (GPa)	$E_{11} = 122;\ E_{22} = E_{33} = 6.2$
	Poisson's ratio (-)	$v_{12} = v_{13} = 0.35;\ v_{13} = 0.5$
	Shear modulus (GPa)	$G_{12} = G_{13} = 3.9;\ G_{23} = 2.1$
Strength	Fiber tensile and compressive (MPa)	$X_t = 1850;\ X_c = 1470$
	Matrix tensile and compressive (MPa)	$Y_t = 29;\ Y_c = 140$
	Shear strength (MPa)	$S_{12} = S_{13} = S_{23} = 65$
Interlaminar properties		
Density (kg/m³)		1200
Elastic modulus (MPa)		$E_n = E_s = E_t = 5000$
Strength properties (MPa)		$t_n = t_s = t_t = 30$
Fracture energy (N/mm)		$G_n^c = 0.6;\ G_s^c = 2.1$

Results and Discussion

This section provides the main results obtained from the LVI simulations conducted on composite laminates. At first, a mesh sensitivity analysis was performed to assure accurate and dependable outcomes. Next, the validation of the proposed damage model, its comparison with existing data, and its ability to accurately capture damage are described. This section examines the influence of damage progression law and impact energy on the projected response. It concludes with an analysis of the observed damage modes.

Mesh sensitivity analysis

The analysis of mesh dependency for the low-velocity impact simulation on composite laminates was performed using an Intel Xeon Dell workstation equipped with 12 CPU cores. The analysis specifically examined the impact energy scenario of 2 J. Figure 2 displays the highest contact force (measured in Newtons) and the amount of time it takes for the central processing unit

(CPU) to complete the task (measured in hours) for different mesh sizes: 0.85 mm, 1 mm, 1.25 mm, and 1.5 mm. The total number of elements varies from 50,476 for the 1.5 mm mesh size to 133,916 for the 0.85 mm mesh size. Significantly, the experiment recorded a maximum contact force of 2238 N, which serves as a standard for evaluating the accuracy of the simulation. The maximal contact force seems to reach a point of convergence between the 1.25 mm and 1.0 mm mesh sizes, with a negligible difference of approximately 5 N. The upper limit of the contact force for the mesh sizes of 1.5 mm and 1.25 mm is around 2400 N, whereas the mesh sizes of 1.0 mm and 0.85 mm exhibit a significantly lower maximum contact value of about 2200 N. This convergence indicates that refining the measurement beyond 1.25 mm does not result in substantial increases in accuracy compared to the experimental value of 2281 N.

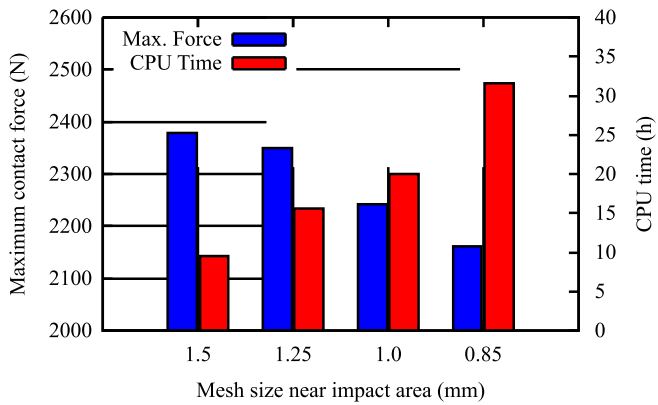

Figure 2: Mesh sensitivity analysis for 2J impact energy using a combination of Puck and GD1

The CPU time exhibits a substantial decrease as the mesh size becomes coarser. More precisely, there is a decrease of approximately five hours in CPU time when comparing a mesh size of 1.0 mm to a mesh size of 1.25 mm. The CPU durations for the 1.5 mm and 1.25 mm mesh sizes range from 10 to 15 hours, whereas the 1.0 mm and 0.85 mm mesh sizes require significantly longer calculation periods of approximately 25 and over 30 hours, respectively. This suggests that using smaller mesh sizes, although they provide slightly more precise results, leads to much higher computational expenses.

Considering the balance between accuracy and computational cost, a mesh size of 1.25 mm appears to be a good choice for further analysis. The 1.25 mm mesh size provides an optimal trade-off between accurately

representing the relevant physics of the simulation and minimising processing time. It closely matches the experimental maximum contact force of 2281 N while yet keeping an acceptable degree of computational efficiency. Hence, for a more in-depth examination, it is advisable to choose the 1.25 mm mesh size as it achieves an excellent compromise between precision and computational effectiveness.

Numerical validation

Figures 3(a), 3(c), and 3(e) demonstrate that both Puck-GD1 and Puck-GD2 simulations accurately represent the overall pattern of the actual data obtained from Feng and Aymerich [31] for all three impact energies (2 J, 4 J, and 8 J). The projected force curves in all the graphs have a comparable form to the experimental curves, characterised by an initial linear increase in force followed by a steady decline. At an impact energy of 2 J, both models closely match the experimental trend. However, Puck-GD2 overestimates the peak contact force, while Puck-GD1 somewhat underestimates it. When the impact energy reaches 4 J, Puck-GD2 persistently overestimates the contact force over the whole impact period, while Puck-GD1 remains more closely aligned but still slightly overestimates it. At the maximum impact energy of 8 J, both models greatly overestimate the peak contact force. However, the Puck-GD2 model deviates more noticeably from the observed curve. The impaction time consistently ranges from 0.004 to 0.005 seconds for all energy levels, suggesting that the simulations accurately represent the timing of the impact event.

In general, the Puck-GD1 and Puck-GD2 simulations provide a fairly accurate representation of the force-time response of composite laminates subjected to low-velocity impacts. Nevertheless, their precision is constrained, particularly in predicting the ultimate force. The rising impact energy trend indicates that the predictive models, particularly Puck-GD2, tend to overestimate the peak contact force to a greater extent at higher energy levels. The overestimation may be attributed to the assumptions and constraints inherent in the Puck failure criteria, which may not adequately consider the intricate damage pathways in composite laminates under greater strain rates. Although Puck-GD1 is generally more precise and dependable in forecasting low-energy impacts, it still exhibits a minor tendency to overestimate at higher energy levels. This indicates that the models accurately capture the fundamental characteristics of the mechanical behaviour of the laminates when exposed to low-velocity impacts, aligning with established principles [16]–[32].

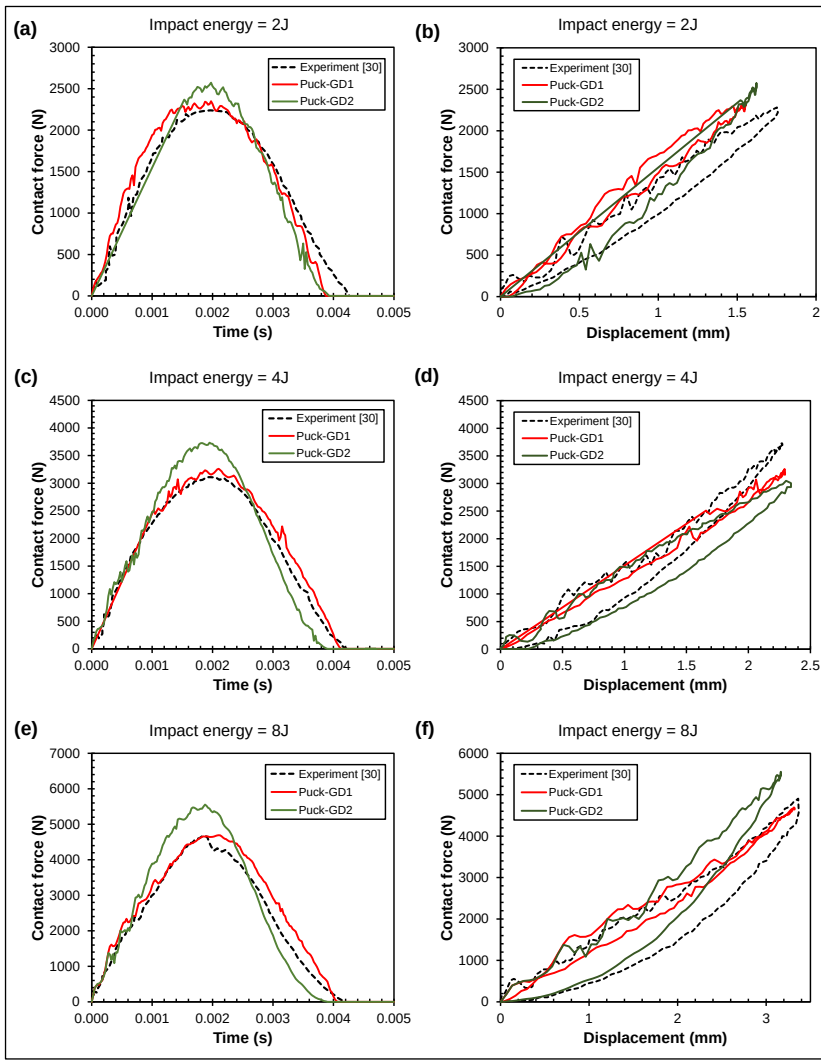

Figure 3: The structural responses of LVI laminate under impact energies (a) – (b) 2 J, (c) – (d) 4 J, and (e) – (f) 8 J

Figures 3(b), 3(d), and 3(f) depict the correlation between predicted force-displacement curves with experimental curves for three impact energies. The quality of the results shown is summarized in Table 8. The overall errors/discrepancies between the simulation and experimental results can be considered reasonably modest, with an approximate range of ±6%. The

differences between the models and the experimental findings indicate that both Puck-GD1 and Puck-GD2 offer quite precise forecasts. Puck-GD1 exhibits slightly smaller discrepancies at lower impact energies, whilst Puck-GD2 has significantly larger inaccuracies at 4 J. The observed trend can be explained by the inherent disparities in the modelling techniques employed by Puck-GD1 and Puck-GD2. Puck-GD1 is more effective in capturing mechanisms related to lower energy absorption, while Puck-GD2's higher error at 4 J suggests susceptibility to complexities associated with mid-range impact energy. In general, both models demonstrate an increase in accuracy as the impact energy rises, suggesting a more reliable capacity to make predictions at higher energy levels. The observed trend aligns with previous research, which has shown that higher energy impacts tend to lead to more predictable and uniform failure modes [30]–[33].

Table 9: Efficiency analysis of energy absorption based on 2 J, 4 J, and 8 J impact energy

Impact energy	Experiment (J)	Puck-GD1 (J)	Error (%)	Puck-GD2 (J)	Error (%)
2 J	2.18	2.00	-5.5	2.05	-3.3
4 J	3.80	3.86	1.6	3.98	4.8
8 J	7.87	7.99	1.5	8.00	1.7

Damage progression mechanism

Figure 4 provides an analysis of inter-fiber failure in tension (IFFT) and compression (IFFC) at different impact energies (2 J, 4 J, and 8 J) using two simulation models: Puck-GD1 and Puck-GD2. In the figure, the red color contour represents the damaged area, while the blue color indicates the undamaged region. An evident finding is that the Puck-GD1 simulations display a smaller region of damage in comparison to Puck-GD2. The distinction can be explained by the intrinsic differences in the criteria for the onset and progression of damage that are incorporated in the two models. Puck-GD1 probably utilises more cautious or stringent criteria for determining failure, which consequently slows down the initiation and spread of damage amongst fibres. On the other hand, Puck-GD2 might utilise more forceful or less limiting measures of damage, resulting in a greater degree of damage under the same impact circumstances.

The progressive increase in the damaged area with an escalating impact energy from 2 J to 8 J is consistent with fundamental principles of material behavior under impact loading. Higher impact energies impart greater stress and strain on the composite material, thereby exceeding the material's threshold for damage initiation and propagation over a more extensive region. This phenomenon aligns with the energy absorption and damage tolerance

characteristics inherent to composite materials, where increased energy input directly correlates with increased damage severity and extent.

Furthermore, the absence of fiber failure (either FFT or FFC) in the simulations suggests that the applied impact energies were insufficient to induce fiber breakage. Fibre failure generally necessitates a greater amount of energy compared to inter-fiber failure, due to the increased strength and rigidity of the fibres in relation to the matrix [20]. The energy levels used (2 J, 4 J, and 8 J) in this study appear to be lower than the crucial threshold required to initiate fibre fracture, leading to the exclusive detection of inter-fiber damage. This discovery is consistent with the results reported in the literature, which suggest that failures in composite laminates under impact loading are mostly caused by the matrix. This is because the matrix has a restricted capacity to absorb and dissipate energy compared to the fibres [16]–[32].

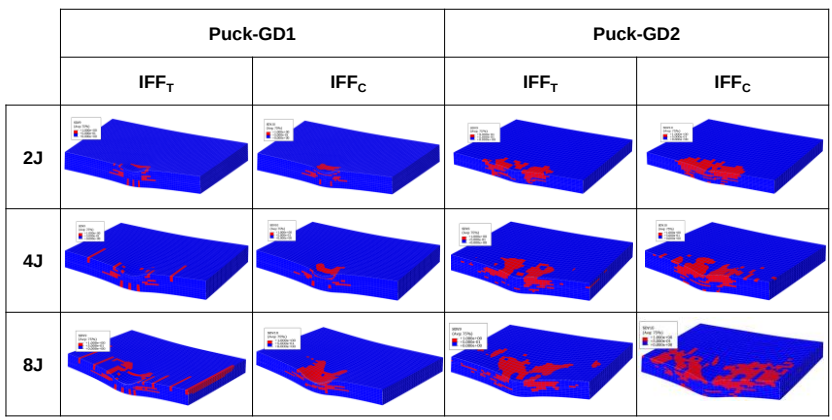

Figure 4: Intralaminar matrix /inter-fiber damage mechanism using Puck-GD1 and GD2 under different impact energies

Figure 5 delineates the delamination patterns at cohesive interfaces within a composite laminate, subjected to 2 J, 4 J, and 8 J impact energies, using the Puck-GD1 simulation model. Again, the delaminated area was highlighted as red, while undamaged areas were coloured blue. The laminate arrangement consists of layers positioned at 0° and 45° angles, which have a substantial impact on how damage is distributed under LVI situations. It can be said that delamination primarily starts and spreads at interfaces where the ply orientations are different. This emphasises the crucial locations that are susceptible to interlaminar stress concentrations.

Examining the area of delamination from cohesive layer 1 (the nearest to the impacted position) to cohesive layer 4 (the furthest from the impacted location) shows a noticeable pattern. At an impact energy of 2 J, delamination is small and negligible in all cohesive layers, except for Coh.1 which exhibits

moderate delamination due to its proximity to the impact site. As the amount of energy exerted increases to 4 J, the area where the material has separated into layers expands, especially at Coh.1 and Coh.2. This suggests that there is a greater capacity for absorbing energy through strain at these interfaces. The impact energy of 8 J leads to extensive delamination throughout all cohesive layers, with notable damage occurring at cohesive layer 1 and 2, and significant spreading towards cohesive layer 3 and 4. This pattern is consistent with the results reported in the literature [31], where larger impact energies are associated with an increase in delamination. This is because the greater energy is dissipated by interlaminar fracture.

As the impact energy increases, the amount and extent of delamination also increase, indicating that the composite material is highly responsive to different levels of low-velocity impact. At energy levels below 2 J, the composite material exhibits localised delamination primarily near the impact zone. Nevertheless, when the impact energy reaches 8J, the delamination not only becomes more widespread but also extends deeper into the laminate. This behaviour is consistent with research on LVI in composites [30]–[34], which indicates that greater impact energy results in broader and more severe delamination. The delamination process is influenced by the increased momentum transfer and subsequent interlaminar stresses. The observed trend, in this case, showcases the composite material's ability to withstand damage, with the Puck-GD1 model accurately depicting the process of delamination under various impact conditions.

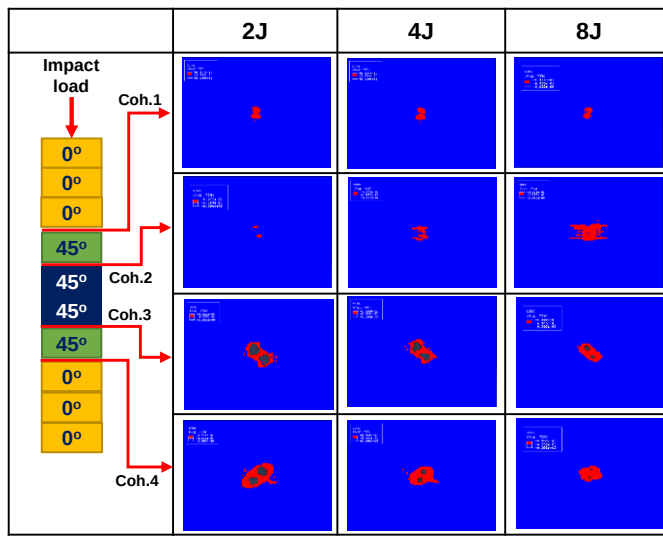

Figure 5: Delamination patterns on cohesive interfaces under different impact energies (2 J, 4 J, and 8 J)

Conclusion

The investigation of composite laminates exposed to LVI has generated significant knowledge of their structural behaviour and failure mechanism. The study employed a 3D finite element model in Abaqus/Explicit, which integrated the VUMAT subroutine, to simulate and analyze the behaviour of composite laminates under varying impact energies (2 J, 4 J, and 8 J). The investigation yields the following conclusions:

a) Applying higher impact energies to the laminate resulted in greater damage and deformation, indicating a higher level of energy absorption.
b) The proposed progression law, specifically gradual degradation, significantly affected energy absorption behavior, allowing for controlled energy dissipation and smoother absorption.
c) Matrix tension failure mode emerged as a crucial dominating factor, resulting in progressive damage accumulation specifically for LVI.

In summary, the study exhibited that the proposed model is appropriate for simulating the failure of laminates, providing valuable guidance for designing advanced composite materials with improved energy absorption and impact resistance for applications in many engineering industries.

Contributions of Authors

The authors confirm the equal contribution in each part of this work. All authors reviewed and approved the final version of this work.

Funding

This work received no specific grant from any funding agency.

Conflict of Interests

One of the authors, Jamaluddin Mahmud is the Editor in Chief of the Journal of Mechanical Engineering (JMechE). The author has no other conflict of interest to note.

Acknowledgement

The authors would like to thank School of Mechanical Engineering, College of Engineering, Universiti Teknologi MARA for providing the facilities and knowledge support.

References

[1] L. Yang, Z. Wu, D. Gao, and X. Liu, "Microscopic damage mechanisms of fibre reinforced composite laminates subjected to low velocity impact", *Computational Materials Science*, vol. 111, pp. 148–156, 2016. https://doi.org/10.1016/j.commatsci.2015.09.039

[2] Y. Tie, T. Sapanathan, M. Rachik, Y. Hou, X. Zhou, and C. Li, "An insight into the low-velocity impact behavior of patch-repaired CFRP laminates using numerical and experimental approaches", *Composite Structures*, vol. 190, pp. 179–188, 2018. https://doi.org/10.1016/j.compstruct.2018.01.075

[3] A. Gliszczynski, "Numerical and experimental investigations of the low velocity impact in GFRP plates", *Composites Part B: Engineering*, vol. 138, no. 1, pp. 181–193, 2018. https://doi.org/10.1016/j.compositesb.2017.11.039

[4] G. Perillo, N. P. Vedvik, and A. T. Echtermeyer, "Numerical analyses of low velocity impacts on composite. Advanced modelling techniques", *Proceedings of the Simulia Community Conference*, pp. 1-16, 2012

[5] J. Zhang and X. Zhang, "An efficient approach for predicting low-velocity impact force and damage in composite laminates", *Composite Structures*, vol. 130, pp. 85–94, 2015. https://doi.org/10.1016/j.compstruct.2015.04.023

[6] L. Maio, E. Monaco, F. Ricci, and L. Lecce, "Simulation of low velocity impact on composite laminates with progressive failure analysis", *Composite Structures*, vol. 103, pp. 75–85, 2013. https://doi.org/10.1016/j.compstruct.2013.02.027

[7] G. Han, Z. Guan, X. Li, and S. Du, "Failure analysis of carbon fiber reinforced composite subjected to low velocity impact and compression after impact", *Journal of Reinforced Plastics and Composites*, vol. 35, no. 9, pp. 727–746, 2016. https://doi.org/10.1177/0731684415627381

[8] P. F. Liu, B. B. Liao, L. Y. Jia, and X. Q. Peng, "Finite element analysis of dynamic progressive failure of carbon fiber composite laminates under low velocity impact", *Composite Structures*, vol. 149, pp. 408–422, 2016. https://doi.org/10.1016/J.COMPSTRUCT.2016.04.012

[9] X. Lou, H. Cai, P. Yu, F. Jiao, and X. Han, "Failure analysis of composite laminate under low-velocity impact based on micromechanics of

failure", *Composite Structures*, vol. 163, no. 12, pp. 238–247, 2016. https://doi.org/10.1016/j.compstruct.2016.12.030

[10] H. Singh, K. K. Namala, and P. Mahajan, "A damage evolution study of E-glass/epoxy composite under low velocity impact", *Composites Part B: Engineering*, vol. 76, pp. 235–248, 2015. https://doi.org/10.1016/j.compositesb.2015.02.016

[11] J. Zhou, B. Liu, and S. Wang, "Finite element analysis on impact response and damage mechanism of composite laminates under single and repeated low-velocity impact", *Aerospace Science and Technology*, vol. 129, p. 107810, 2022. https://doi.org/10.1016/j.ast.2022.107810

[12] O. Falcó, C. S. Lopes, D. E. Sommer, D. Thomson, R. L. Ávila, and B. H. A. H. Tijs, "Experimental analysis and simulation of low-velocity impact damage of composite laminates", *Composite Structures*, vol. 287, no. 7-8, p. 115278, 2022. https://doi.org/10.1016/J.COMPSTRUCT.2022.115278

[13] W. Ao, W. Zhuang, B. Xing, Q. Zhou, and Y. Xia, "Finite element method of a progressive intralaminar and interlaminar damage model for woven fibre laminated composites under low velocity impact", *Materials & Design*, vol. 223, no. 1, p. 111256, 2022. https://doi.org/10.1016/J.MATDES.2022.111256

[14] S. Joglekar, V. Ranatunga, and M. Pankow, "Validation of an efficient finite element analysis approach for simulation of low velocity impact and compression strength after impact response", *Composite Structures*, vol. 255, no. 15, p. 112945, 2020. https://doi.org/10.1016/J.COMPSTRUCT.2020.112945

[15] M. H. Nagaraj, E. Carrera, and M. Petrolo, "Progressive damage analysis of composite laminates subjected to low-velocity impact using 2D layer-wise structural models", *International Journal of Non-Linear Mechanics*, vol. 127, p. 103591, 2020. https://doi.org/10.1016/J.IJNONLINMEC.2020.103591

[16] M. S. Meon, N. H. M. Nor, S. Shawal, J. B. Saedon, M. N. Rao, and K.-U. Schröder, "On the Modelling Aspect of Low-Velocity Impact Composite Laminates", *Journal of Mechanical Engineering*, vol. 17, no. 2, pp. 13–25, 2020. https://doi.org/10.24191/jmeche.v17i2.15297

[17] J. Zhou, P. Wen, and S. Wang, "Numerical investigation on the repeated low-velocity impact behavior of composite laminates", *Composites Part B: Engineering*, vol. 185, no. 8, p. 107771, 2020. https://doi.org/10.1016/J.COMPOSITESB.2020.107771

[18] S. Sridharan and M. Pankow, "Performance evaluation of two progressive damage models for composite laminates under various speed impact loading", *International Journal of Impact Engineering*, vol. 143, no. 2, p. 103615, 2020. https://doi.org/10.1016/J.IJIMPENG.2020.103615

[19] Y. Zhao and X. Zhou, "Numerical analysis of unidirectional carbon-fibre/epoxy composite laminates under low velocity impacts of different forms", *Computational Materials Science*, vol. 231, p. 112611, 2024. https://doi.org/10.1016/j.commatsci.2023.112611

[20] N. Mohamad, M. Meon, N. Mohamad Nor, S. Shawal, J. Saedon, M. Rao, and K. Schröder, "Modelling Low-Velocity Impact on Composite Laminate Considering Inter-and Intralaminar Damage", *Proceedings of International Exchange and Innovation Conference on Engineering & Sciences*, vol. 5, pp. 63–66, 2019. https://doi.org/10.15017/2552938

[21] J. Zhou, P. Wen, and S. Wang, "Finite element analysis of a modified progressive damage model for composite laminates under low-velocity impact", *Composite Structures*, vol. 225, no. 8, p. 111113, 2019. https://doi.org/10.1016/J.COMPSTRUCT.2019.111113

[22] X. Li, D. Ma, H. Liu, W. Tan, X. Gong, C. Zhang, and Y. Li, "Assessment of failure criteria and damage evolution methods for composite laminates under low-velocity impact", *Composite Structures*, vol. 207, pp. 727–739, 2019. https://doi.org/10.1016/j.compstruct.2018.09.093

[23] B. B. Liao and L. Y. Jia, "Finite element analysis of dynamic responses of composite pressure vessels under low velocity impact by using a three-dimensional laminated media model", *Thin-Walled Structures*, vol. 129, pp. 488–501, 2018. https://doi.org/10.1016/J.TWS.2018.04.023

[24] B. B. Liao, H. C. Tan, J. W. Zhou, and L. Y. Jia, "Multi-scale modelling of dynamic progressive failure in composite laminates subjected to low velocity impact", *Thin-Walled Structures*, vol. 131, pp. 695–707, 2018. https://doi.org/10.1016/J.TWS.2018.07.047

[25] Z. Hashin, "Failure Criteria for Unidirectional Fiber Composites", *Journal of Applied Mechanics*, vol. 47, no. 2, pp. 329–334, 1980

[26] S. Long, X. Yao, and X. Zhang, "Delamination prediction in composite laminates under low-velocity impact", *Composite Structures*, vol. 132, pp. 290–298, 2015. https://doi.org/10.1016/j.compstruct.2015.05.037

[27] J. Du, Y. Tie, C. Li, and X. Zhou, "Numerical and experimental study for damage characterization of composite laminates subjected to low-velocity impact", *Materials Physics and Mechanics*, vol. 27, pp. 195–204, 2016

[28] A. Puck and H. Schürmann, "Failure analysis of FRP laminates by means of physically based phenomenological models", *Composites Science and Technology*, vol. 62, pp. 1633-1662, 2002. https://doi.org/10.1016/S0266-3538(01)00208-1

[29] C. S. Lee, J. H. Kim, S. K. Kim, D. M. Ryu, and J. M. Lee, "Initial and progressive failure analyses for composite laminates using Puck failure criterion and damage-coupled finite element method", *Composite Structures*, vol. 121, pp. 406–419, 2015. https://doi.org/10.1016/j.compstruct.2014.11.011

[30] J. R. Shao, N. Liu, Z. J. Zheng, and Y. Yang, "Elastic-plastic progressive damage model and low-velocity impact failure mechanism of composite materials", *Materials Today Communications*, vol. 31, p. 103685, 2022. https://doi.org/10.1016/j.mtcomm.2022.103685

[31] D. Feng and F. Aymerich, "Finite element modelling of damage induced by low-velocity impact on composite laminates", *Composite Structures*, vol. 108, pp. 161–171, 2014. https://doi.org/10.1016/j.compstruct.2013.09.004

[32] H. Tuo, Z. Lu, X. Ma, J. Xing, and C. Zhang, "Damage and failure mechanism of thin composite laminates under low-velocity impact and compression-after-impact loading conditions", *Composites Part B: Engineering*, vol. 163, pp. 642–654, 2019. https://doi.org/10.1016/j.compositesb.2019.01.006

[33] Y. Kumar, M. Rezasefat, S. C. Amico, A. Manes, P. I. Dolez, and J. D. Hogan, "Comparison of two progressive damage models for predicting low-velocity impact behavior of woven composites", *Thin-Walled Structures*, vol. 197, no. 7, p. 111611, 2024. https://doi.org/10.1016/j.tws.2024.111611

[34] J. R. Shao, N. Liu, and Z. J. Zheng, "A modified progressive damage model for simulating low-velocity impact of composite laminates", *Advances in Mechanical Engineering*, vol. 14, no. 5, pp. 1–16, 2022. https://doi.org/10.1177/16878132221095948